Geophysical Research Letters

RESEARCH LETTER
10.1029/2018GL079665

Near-Surface Environmentally Forced Changes in the Ross Ice Shelf Observed With Ambient Seismic Noise

J. Chaput[1,2], R. C. Aster[3], D. McGrath[3], M. Baker[3], R. E. Anthony[4], P. Gerstoft[5], P. Bromirski[5], A. Nyblade[6], R. A. Stephen[7], D. A. Wiens[8], S. B. Das[7], and L. A. Stevens[9]

[1]Department of Mathematics, Colorado State University, Fort Collins, CO, USA, [2]Department of Geological Sciences, University of Texas at El Paso, El Paso, TX, USA, [3]Department of Geosciences, Colorado State University, Fort Collins, CO, USA, [4]U.S. Geological Survey, Albuquerque Seismological Laboratory, Albuquerque, NM, USA, [5]Scripps Institution of Oceanography, University of California, San Diego, La Jolla, CA, USA, [6]Department of Geosciences, Pennsylvania State University, State College, University Park, PA, USA, [7]Woods Hole Oceanographic Institution, Woods Hole, MA, USA, [8]Department of Earth and Planetary Sciences, St. Louis, MO, USA, [9]Lamont-Doherty Earth Observatory, Columbia University, Palisades, NY, USA

Key Points:
- High-frequency (>5 Hz), narrow-band signals observed on an ice shelf are sensitive to changes in the near-surface firn layer
- Spectral peak frequency changes coincide with melt/freeze events on the ice shelf as well as with storm-driven redistribution snow
- Melt events have a unique spectral signature and can be modeled in terms of the penetration depth to which these thermal anomalies diffuse

Supporting Information:
- Supporting Information S1

Correspondence to:
J. Chaput,
jchaput82@gmail.com

Citation:
Chaput, J., Aster, R. C., McGrath, D., Baker, M., Anthony, R. E., Gerstoft, P., et al. (2018). Near-surface environmentally forced changes in the Ross Ice Shelf observed with ambient seismic noise. *Geophysical Research Letters*, *45*. https://doi.org/10.1029/2018GL079665

Received 18 JUL 2018
Accepted 15 AUG 2018

Abstract Continuous seismic observations across the Ross Ice Shelf reveal ubiquitous ambient resonances at frequencies >5 Hz. These firn-trapped surface wave signals arise through wind and snow bedform interactions coupled with very low velocity structures. Progressive and long-term spectral changes are associated with surface snow redistribution by wind and with a January 2016 regional melt event. Modeling demonstrates high spectral sensitivity to near-surface (top several meters) elastic parameters. We propose that spectral peak changes arise from surface snow redistribution in wind events and to velocity drops reflecting snow lattice weakening near 0°C for the melt event. Percolation-related refrozen layers and layer thinning may also contribute to long-term spectral changes after the melt event. Single-station observations are inverted for elastic structure for multiple stations across the ice shelf. High-frequency ambient noise seismology presents opportunities for continuous assessment of near-surface ice shelf or other firn environments.

Plain Language Summary Ice shelves are the floating buttresses of large glaciers that extend over the oceans and play a key role in restraining inland glaciers as they flow to the sea. Deploying sensitive seismographs across Earth's largest ice shelf (the Ross Ice Shelf) for 2 years, we discovered that the shelf nearly continuously *sings* at frequencies of five or more cycles per second, excited by local and regional winds blowing across its snow dune-like topography. We find that the frequencies and other features of this *singing* change, both as storms alter the snow dunes and during a (January 2016) warming event that resulted in melting in the ice shelf's near surface. These observations demonstrate that seismological monitoring can be used to continually monitor the near-surface conditions of an ice shelf and other icy bodies to depths of several meters.

1. Introduction

Ice shelf weakening or collapse increases the flux of grounded glacial ice to the ocean, thus contributing to global sea level rise. Widespread and accelerating mass losses from Antarctica (Paolo et al., 2015; Pritchard et al., 2012; Rignot et al., 2013; Shepherd, 2018) are being driven by thinning and retreat of ice shelves, providing clear motivation for improved monitoring and understanding of ice shelf changes across all relevant temporal and spatial scales. This includes a strong impetus to observe and better understand near-surface snow and firn behavior through annual and short-term melt, compaction, and accumulation cycles (J. Li & Zwally, 2011; Reeh, 2008) given its relevance to ice shelf stability and to estimating remotely sensed volume to mass conversions (e.g., ICESat-1 and 2). Antarctic ice shelves are vulnerable to both oceanographic (Alley, Scambos, Anderson, et al., 2018; Cathles et al., 2009; Pritchard et al., 2012) and atmospheric (Alley, Scambos, Miller, et al., 2018; Holland et al., 2015) perturbations. Although preconditioning processes may operate over decadal time scales, total or partial ice shelf collapse can occur suddenly, with loss of shelf buttressing leading to increased rates of ice flux across the grounding line (Furst et al., 2016; Pritchard et al., 2012; Rignot et al., 2004; Scambos et al., 2004) with dynamic thinning possible far inland (Reese et al., 2018). Ice shelves can be desta-

bilized by a variety of factors, including increased surface melt, ponding and hydrofracture (Alley, Scambos, Miller, et al., 2018; Hubbard et al., 2016), propagation of rifts that cross the compressive arch (Doake et al., 1998), and elevated basal melt rates (Pritchard et al., 2012). Conversion of permeable, cold firn surfaces to impermeable superimposed ice surfaces as melt seasons intensify leads to surface ponding and hydrofracture, which are both critical processes in ice shelf destabilization, and were integral to the rapid collapse of Larsen B in 2004 (Alley et al., 2016; Banwell et al., 2013; Kuipers Munneke et al., 2017; Kulessa et al., 2014; McGrath et al., 2012; Scambos et al., 2009).

We present high-frequency single-station ambient seismic observations from the Ross Ice Shelf (RIS) that show impacts of environmental forcing on both rapid (hours) and slow (months) time scales. Pervasive station-specific patterns of time-dependent spectral peaks (referred to as spectral resonances here) are observed at all seismic stations on the RIS, and we demonstrate that spectral peak patterns can be inverted to estimate physical changes in near-surface (~5 m) snow and firn structure. We also show that effects due to wind and storm forcing are distinct from those of surface air temperature changes and near-surface melting. In particular, we show the following: (1) The observed *resonances peaks* are not true resonances like normal modes or H/V amplifications but are a consequence of discrete spatial coupling of wind with semiperiodic surface structures such as dunes and sastrugi combined with an extremely low seismic velocity firn structure. (2) Strong wind events may rapidly alter surface bedform structures, resulting in smooth shifts of frequency peaks as wind events taper. This effect is caused by a combination of direct snow deposition and the creation of bedform structures that alter the spatial coupling of wind with the snow surface. (3) Melt-related forcing can be unambiguously observed and typically results in a smooth downward shift of various resonance peaks as near-zero degree Celsius temperatures diffuse to depth and weakens the near-surface snow matrix.

2. Firn-Trapped Resonance Modes

The RIS project incorporated 34 broadband seismic stations that spanned the ice shelf in two transects (Figure 1a). This effort was motivated by a gap in our understanding of how ice shelves respond to oceanic, atmospheric, elastic, and gravity waves at frequencies and wavenumbers relevant to evolution and stability (Bromirski et al., 2010; Chen et al., 2018; Pritchard et al., 2012; Sergienko, 2010) and to extend tomographic and seismic source studies in the region. Although relatively stable in recent studies of ice mass loss when compared to other ice shelves in West Antarctica that have become strongly impacted by enhanced basal melt rates (e.g., Dotson and Getz ice shelves), the RIS has exhibited recent changes in seasonal ice mass balance that may herald a departure from this historic stability (Hulbe et al., 2016; Marsh et al., 2016; Paolo et al., 2015). Periodic collapses of the West Antarctic Ice Sheet have coincided with the disappearance of buttressing ice shelves and by the emergence of open waters in the Ross Sea embayment (Naish, 2009).

RIS seismic stations are recorded continuously at sampling rates of 100 or 200 Hz between November 2014 and February 2017. The high-frequency (above 5 Hz) ambient seismic wave field on the RIS was observed to contain persistent and time-varying spectral resonances. At these frequencies, seismic signals are highly sensitive to near-surface snow and firn properties. Generally, we observed strong year-round and time-varying spectral peaks between ~4 and 50 Hz (Figure 1b), superimposed upon more stable, lower frequency thin plate elastic modes described elsewhere (Suppl. S2, Bromirski & Stephen, 2012; Chen et al., 2018; Fretwell et al., 2013; Stahler et al., 2017; Xie & Farmer, 1994; Zhan et al., 2014; Figures S1c and S2).

We observed both gradual (on the scale of months) and rapid (on the scale of hours) spectral peak amplitude and frequency changes, which included excursions of up to several hertz. We also resolved widespread anisotropic mode splitting (Aster et al., 1990) in horizontal seismogram components that is consistent with previously recognized ~5% N-S (slow) and E-W (fast) S-wave anisotropy in the shallow RIS (Figure S1d, Diez et al., 2016; Humbert et al., 2005; Walker et al., 2013). The systematic observation of ice shelf seismic anisotropy helped confirm that the phenomenon is due to shallow RIS structure and is not simply an artefact of previously identified noise sources in the Antarctic such as wind coupling with local structures or temperature dependent instrumentation noise (Anthony et al., 2015; Suppl. S1, MacAyeal et al. 2006). Semichaotic high-frequency (above ~5 Hz) spectral peaks were previously noted by Bromirski and Stephen (2012) at near-ice edge stations from the Nascent Iceberg experiment, which featured radically different instrumentation. Finally, a ~5-km aperture short period seismic array deployed for 2 weeks near station DR10 in 2014 (Diez et al., 2016), which featured entirely different seismometers, data loggers, and (very small and near-surface) solar panel systems

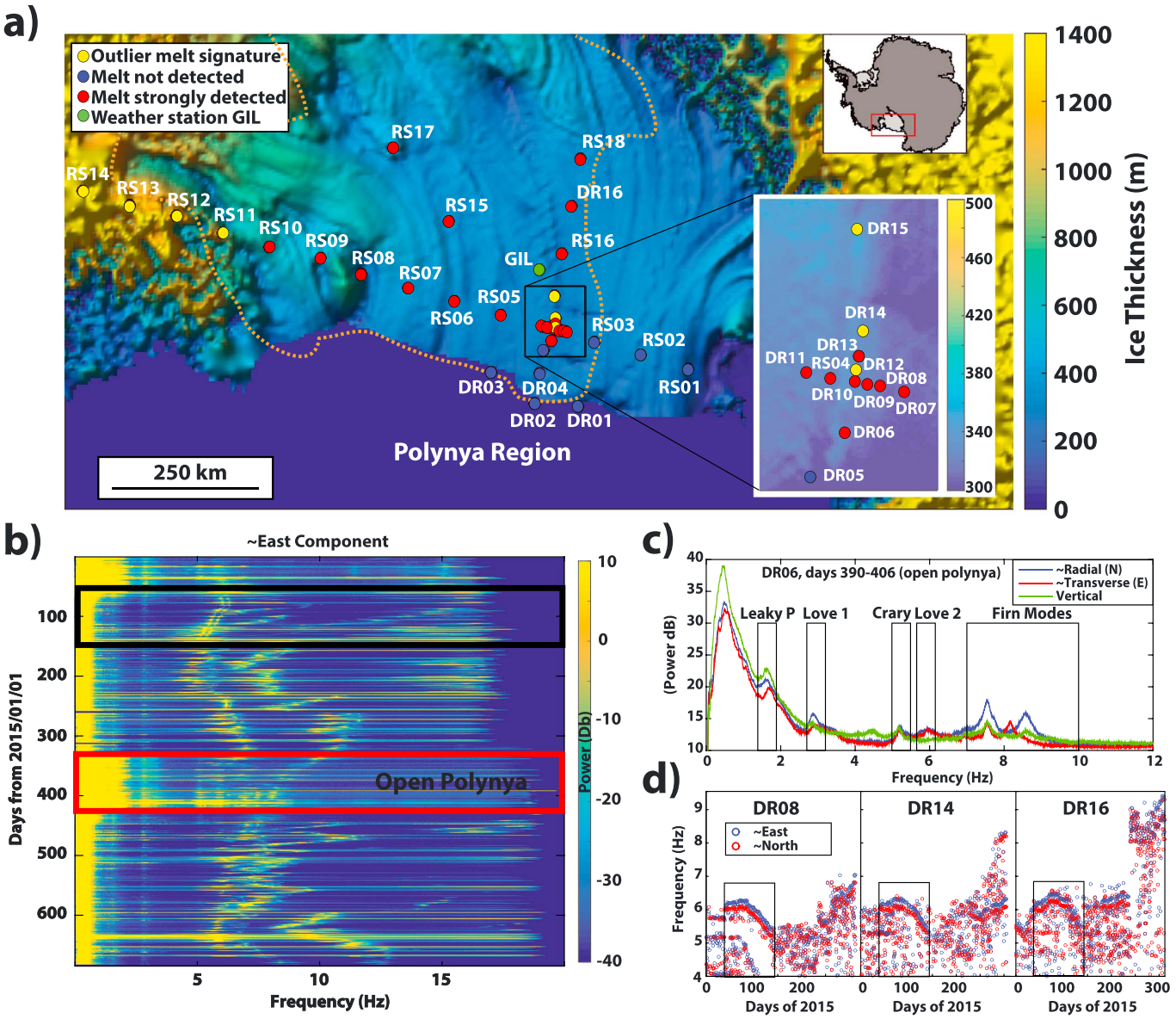

Figure 1. (a) RIS seismic array (Bromirski et al., 2015) overlaid on BEDMAP2 (Fretwell et al., 2013) derived ice thicknesses. Station colors depict whether or not the prominent 2016 melt event was detected via spectral peak variations (see Figures 2b and 2c) and does not necessarily relate to the presence of melt-related layers identified in snow pits, as explained in Figure 3. Stations exhibiting the most common spectral response to the melt event as shown in Figures 2b and 2c are labeled as *melt strongly detected*, while uncharacteristic but evident responses are noted as *outlier melt signature*. The orange contour approximates the region of surface melt during this period (Nicolas et al., 2017), characterized as areas that experienced at least 13 days of abnormally warm surface air temperatures (for enlarged version, see supporting information Figure S15). (b) Two years of representative spectral resonances at station DR06 assemble via multitaper spectral estimate (Park et al., 1987). This behavior was observed across all three components. RIS plate modes (Chen et al., 2018) were stable in frequency with higher amplitudes during times when the ice front polynya was present (red box; Bromwich et al., 2013; Fetterer et al., 2002; Peterson, 1993) and when sea ice did not directly abut the ice shelf (see Figure S2), while the highly variable high-frequency firn modes could generally be observed throughout the year. The black box is referred to in (d). (c) Average spectral power for periods when the RIS ice front polynya was open (red box time period shown in panel b), showing various plate modes (denoted as (1) Leaky-P, (2) Fundamental Love, (3) First Love, (4) Fundamental Crary 1, and (5) firn modes. (d) Representative examples of firn anisotropy (Diez et al., 2016), indicated by the spectral offset in North and East components. The circles correspond to tracked peaks for the North and East components, and allow for direct overlay comparison of spectra. The black boxes in (b) and (d) correspond to the same particularly stable and obvious case of this anisotropy. The variability and magnitude of this splitting between ~North and ~East components is the subject of ongoing work. RIS = Ross Ice Shelf.

recorded similar modal spectra (peaks near 20 Hz) as DR10, and at amplitudes that indicate that DR10 was not the source of this excitation (see section 1 in supporting information, Figure S16).

Strongly horizontally polarized particle motions (which exhibit typical linearity values near 0.9, as quantified by particle motion eigenvalue ratios; Aster et al., 1990, Figure S6) lead us to interpret these modes as a superposition of fundamental and higher-order Rayleigh waves (e.g., Sezawa waves; Kushibiki et al., 1990; Mohanan et al., 2013) and, potentially, shallow Love waves. The strong velocity gradient of the near-surface ice shelf (i.e., P-wave velocity ranging from 100 and 3,000 m/s over tens of meters; Diez et al., 2016), numerous shallow velocity reversals, and local lateral homogeneity produce a near-surface waveguide that sustains these modes in Antarctic glacial environments (Albert, 1998; Anthony et al., 2015). We note in passing that this surface-bounded waveguide system has analogies to those exploited for Surface Acoustic Wave devices in thin film engineering applications, where surface waves are noted to be sensitive to minute changes in near-surface properties (Glushkov et al., 2012; Mohanan et al., 2013; Rodriguez-Madrid et al., 2012). Although direct phase velocity measurements were not available at these frequencies in the RIS data due to the large station spacings (>5 km), observed and modeled spectral and environmental sensitivities, as shown below, are consistent with this interpretation.

2.1. Surface Environmental Forcing from Wind and Temperature

Spectral peak frequency shifts on time scales as rapid as a few hours were strongly correlated with regional wind events (Figures 2a and 2b). We constrained regional wind activity using a central RIS located Automatic Weather Station (GIL; Matthew et al., 2012; Figure 1a) and correlated this metric with spectral power at RIS stations between 3 and 20 Hz (e.g., DR06, Figure S8a).

Spectral power and wind speeds were highly correlated at zero time offset (Figures S8b and S8c), and many spectral peak shifts were strongly associated with wind events. The onset of strong wind typically resulted in an immediate downward shift in peak frequency accompanied with an increase in spectral power, followed by a peak frequency increase as wind speed decreased. The recovered modal frequency following wind events sometimes exceeded the prestorm peak values, indicating that a seismically observable near-surface change had occurred.

Seismically observable temporal changes of hours to days occurring in the absence of wind activity were found to be associated with temperature changes (Figure 2c). An especially interesting example is a widespread ($\approx 8 \times 10^5$ km^2) melt event attributed to strong El Niño forcing that occurred on the central RIS during January 2016 (Nicolas et al., 2017; Figure 1a). Automatic weather station temperatures (collected on raised towers; Matthew et al., 2012) for this melt event approached 0°C over an extended region, with only brief excursions above freezing, so the amount of melt within the firn column was limited.

Laboratory experiments (Takei & Maeno, 2004) have demonstrated that Poisson's ratio, Young's modulus, and seismic wave velocities in porous snow can drop due to softening by as much as 35% as the system warms to between −1°C and −0.1°C in the absence of melting, compaction, or percolation. Assuming no substantial structural changes during the first few days of the melt event (i.e., small degree of concurrent melting and compaction), a near-surface reduction in elastic moduli predicts a gradual downward shift in modal frequencies, with detailed behavior depending on the time-dependent depth profile of the temperature change. Qualitatively, a consistent spectral evolution was observed at the majority of stations that experienced surface melt as mapped by Nicolas et al. (2017). We highlight here representative cases (Figures 2c and 2d, DR08, DR09, DR13, RS06, RS09) and show results for all stations Figure S13. Notably, the early partial recovery to the premelt response at DR08 (also seen at DR13) coincided with the first substantial postevent temperature decrease recorded at GIL (Day 22, Figure 2d; Cold Snap), suggesting rapid temperature-driven firn weakening followed by strengthening. Persistent changes in resonance patterns after the melt additionally imply a long-term change in shallow structure. Strong wind was absent during the postmelt period.

2.2. Interpretation of Wind-Forced Spectral Changes

We isolated a representative sequence of three wind events in 2015 during which sustained wind speeds exceeded 20 m/s at GIL (Figures 2a and 2b) and examined hourly spectrograms and particle motions for a 15-day period encompassing each event at station (DR06). In all three cases, the onset of strong local wind resulted in a contemporaneous decrease and broadening of spectral peaks (Figure S6a), followed by a rapid (~1 Hz/hr) frequency increase at the end of the event. The relative amplitudes of various frequency peaks also varied somewhat, but this effect was not studied further. This trio of events was followed by a low-wind

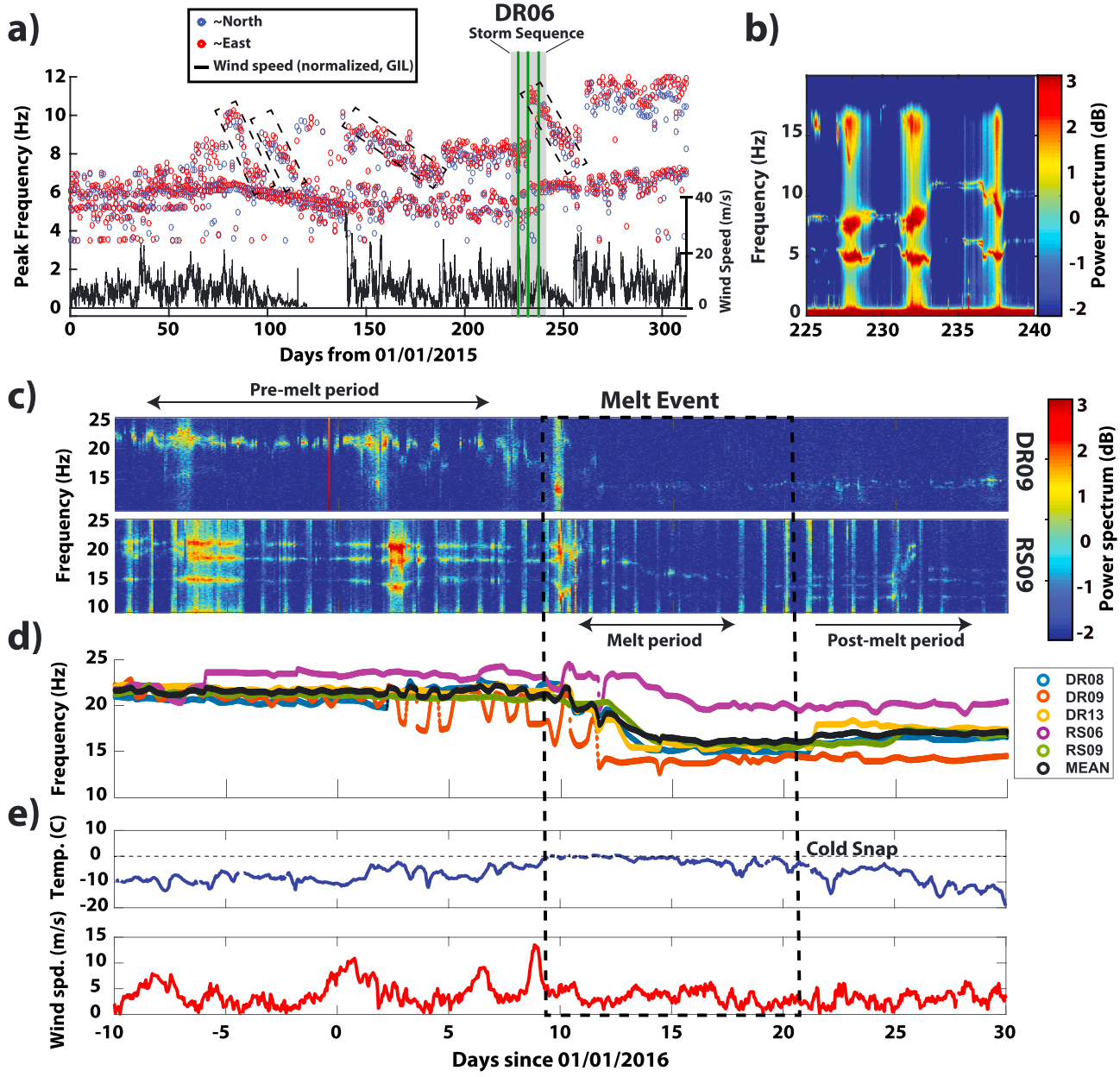

Figure 2. (a) Spectral peak tracking at DR06 for the first 312 days of 2015 compared with wind speed at weather station GIL (Figure 1a). Vertical green lines depict three strong wind events that are analyzed in detail in further panels, and the black boxes show periods of spectral decay associated with proposed slow erosion of surface dune or sastrugi structures. (b) High-resolution spectrogram for a period encompassing three prominent wind events in (a), the second of which results in a significant increase in spectral content. Poststorm upward shifts occur extremely rapidly, on the scale of a few hours (not to be confused with the long spectral decay that occurs in the subsequent months). (c) Spectrograms at two Ross Ice Shelf stations that show similar behavior, encompassing a widespread melt event in January 2016. Periods during which the spectrum was averaged for the associated structural inversion (Figure 3b) are noted as *premelt period* and *melt period*, and a return to typical subfreezing temperatures is noted by *postmelt period*. Periodic broadband pulses (e.g., RS09) are hypothesized to be a consequence of tidal currents or other forcing, but are not addressed in this paper and are not associated with the spectral peak changes discussed here. (d) Superimposed peak-tracked spectral signatures at 5 stations, along with the average, denoted by the black trace, showing highly similar spectral responses to the melt event, and showing a 2- to 4-day onset delay. (e) Wind speed and air temperature recorded at station GIL. The first significant return to colder temperatures is noted as *cold snap* and results in a modest up-tick in frequency content at these Ross Ice Shelf stations.

period, during which we observed a slower frequency decrease for the higher of two principal frequency peaks (Figure 2a) at a rate of ~3–4 Hz/month. The first and third wind events in this series showed a poststorm peak frequency recovery to nearly prestorm conditions. However, the second event induced an abrupt (over several hours) increase near the end of the wind event of ~3 Hz in a higher mode, reaching a frequency that exceeded its prestorm value. A similar effect was also observed, but to a lesser degree, at other regional stations (e.g., RS04) for this event.

Rapid peak frequency shifts during and after wind events may illuminate mode sensitivity to source coupling variations reflecting changing surface conditions, whereas the long-term postevent frequency shift during periods of lower wind is indicative of a sustained near-surface structural change. Candidate near-surface mechanisms that are consistent with a poststorm increase in peak frequency include a thickness change in the uppermost strata (via deposition or erosion), strain weakening/hardening, or gradual changes in local drift topography that modify the spatial surface wind coupling. The Antarctic Ice Sheet hosts a plethora of semiperiodic surface structures such as sastrugi, Barchan dunes, Whaleback dunes, and megadunes, spanning multitudes of scales and surface reliefs (Dadic et al., 2013; Ekaykin et al., 2016; Filhol & Sturm, 2015). These features may have heights of several meters and length scales of several to 10s of meters, though Barchan dunes have typically much smaller vertical relief. Whaleback dunes consist of high-relief accumulations that form during high wind speeds (>15 m/s) and are noted for being bedforms that occur during especially strong storm events. Kochanski et al. (2018) usefully outline statistical distributions of various alpine surface snow features for the Front Range Mountains (CO, USA), but it is unclear to what extent these characterizations are suitable for the RIS.

The drifting snow budget can vary dramatically within storms in response to small fluctuations in wind speed (1–2 m/s), and the transport threshold is sharp and dependent on multiple factors (Sommer et al., 2018), such as wind strength and the presence and character of freshly deposited snow. This may explain why the first and third wind events in Figure 2b do not cause large frequency peak shifts upon termination, while the second shows a dramatic effect. The addition of time-lapse photography would be a useful supplement to future studies to help illuminate the nature and evolution of these snow bedforms. Preconditioning probably also plays a role, in that sintered snow may require particularly strong winds to generate a drifting snow budget, whereas fresh deposits may respond to much weaker wind events (L. Li & Pomeroy, 1997). For instance, the lower tracked spectral peak in Figures 2a and S8a undergoes a period of relative stability between Days 0 and 140, during which multiple storm events appear to have little impact on its behavior. The largest recorded spectral power spike of that year on Day 140, however, (corresponding locally to the highest wind speed, given correlations in Figure S8c) broke this stability, and subsequent wind events induced strong spectral shifts.

Interpretation of wind events has an additional complexity beyond structural changes induced by drifting snow or ablation in that variations in the spatial distribution of wind coupling surface seismic sources may also produce spectral peak amplitude changes and/or shifting for a constant subsurface velocity structure (Figure S9). Such a process might ensue from the creation of quasi-periodic drift structures as drifting snow is deposited as a function of tapering wind. In this scenario, a slow recovery of the seismic spectrum to the predrifting state may occur if drift topography is subsequently reduced via low-wind erosion and/or surface sublimation (Van den Broeke, 1997; Van Lipzip et al., 2004). The slow decrease (over months) in frequency of the higher peak after the third storm in Figure 2a may reflect a transition from a deposition/formation regime for dunes (during and directly poststorm) to an erosion/sublimation regime that occurs during protracted low-wind periods. This provides a hypothesis for how some lower frequency peaks (~5 Hz), featuring wave modes that are sensitive to greater depths, but also sources at greater distances, are also affected.

2.3. Inversion of 2016 Melt Event-Induced Spectral Changes

Modeling and inversion of shallow RIS seismic structure changes driven by temperature and melt first requires estimation of a prechange baseline velocity model. Power spectral inversion is expected to be nonunique (Piña-Flores et al., 2016), so a Bayesian approach was applied to thoroughly explore the model space. A 1-D Markov Chain Monte Carlo seismic structure inversion was performed using the OASES elastic waveguide modeling package for horizontally layered media (Schmidt and Jensen, 1985; see supporting information S1). Initial velocity models at representative stations were estimated using averaged spectral data for the 15-day period preceding the melt event (Figure 2c). Marginal posterior distributions for P- and S-wave velocities (V_p, V_s) at representative station DR09 are shown in Figure 3a, along with a random subset of power spectra chosen from the posterior distribution (Figure 3b).

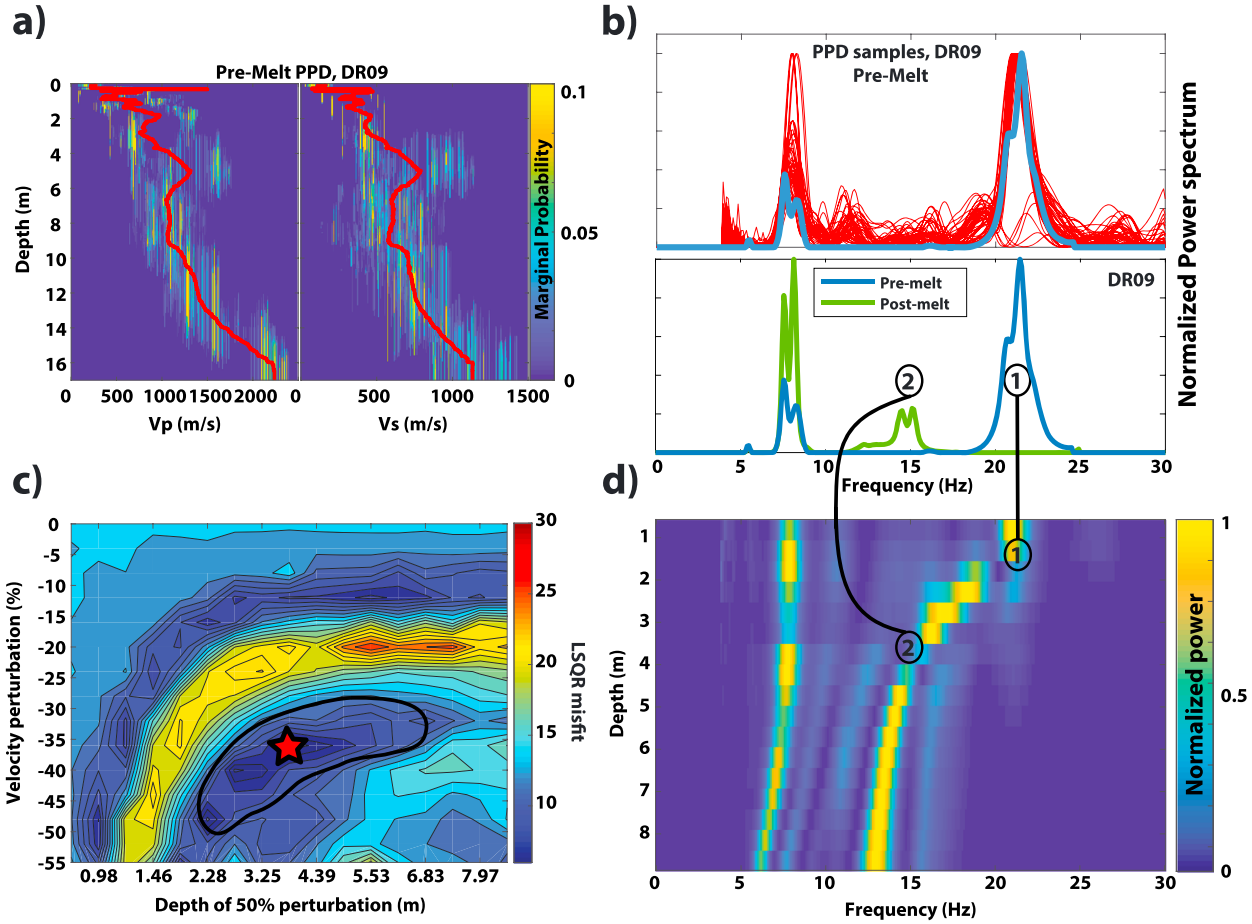

Figure 3. (a) Marginal PPD for V_p and V_s for the premelt resonances at station DR09, obtained by MCMC inversion of power spectra (See Suppl. S4: 1-D MCMC inversion, Capelli et al., 2016). The red curves indicate the marginal posterior mean for P and S velocities. (b) Top panel, representative subset of power spectral models (red curves) from the PPD in (a) for station DR09, compared with the observed premelt spectrum (blue curve). Bottom panel, averaged observed premelt and postmelt spectral resonances (blue and green curves, respectively) at DR09. **(1)** and **(2)** indicate the position of a higher frequency peak of interest before and after the melt event. (c) Contour plot depicting a grid search of penetration depth versus velocity perturbation applied to the premelt model (peak pattern **(1)**, in b), and fit to the postmelt resonance peak pattern, as denoted by peak pattern **(2)** in (b), lower panel. The minimum with respect to a least squares fit is represented by the red star, denoting a 35–40% perturbation with a depth penetration of 3–4 m. The premelt model used here is the mean posterior model shown in (a). (d) Example frequency peak response to a 40% velocity drop with varying degrees of depth penetration for the DR09 premelt velocity model in (a). Note that lower frequency spectral peaks can be nearly unaffected if the perturbation depth is shallow. **(1)** and **(2)** denote observed premelt and postmelt peaks plotted in (b). PPD = Posterior Probability Distributions; MCMC = Markov chain Monte Carlo.

We utilized the maximum a posteriori model from the above procedure as a premelt reference model and applied a velocity perturbation to the near surface weighted by a depth-dependent error function to best model the shifts in resonance patterns induced during the 2016 melt event. For stations that exhibited the relatively simple behavior shown in Figures 2c and 2d, the downward shift in resonances can be explained by a velocity drop of ~35% with a depth kernel length scale of a few meters. This response is consistent with experimental estimates of Takei and Maeno (2004) for mechanical properties of snow undergoing temperature changes just below the melting point. The diffusion depth scale suggested in Figure 3c is further supported by Gilbert et al. (2014), where a parameterized surface energy balance model was implemented to model firn temperature profile responses to changes in surface heating and cooling at the Col du Dome in the French Alps. For persistent near 0°C air temperature forcing, a temporally damped response of 2–4 days was both modeled and observed in their study, thus yielding both depth penetration of the thermal forcing and the corresponding time scale over which this diffusion occurred. For RIS stations at which the melt event was detected, a similar time scale of 2–4 days was observed before spectral peak patterns stabilized (Figures 2d and S12). This observation suggests that a similar time scale and depth penetration of the surface thermal anomaly into the RIS firn may also be applicable.

The modal response to the velocity decrease noted in Figure 3c was consistent across a number of structural models selected from the posterior of the premelt power spectrum (more robust in frequency shift value than peak amplitude; Figure S11), indicating that although the posterior distribution for structural inversion may have multiple optimal solutions, these models responded similarly to velocity perturbations. Although the relative amplitude of frequency peaks varied substantially in the model space, the phase error (i.e., the expected shift of a given peak as a response to a velocity perturbation) was sharply contained within ± 1 Hz within its 95% confidence interval, indicating a small error in terms of a velocity perturbation estimate. This is not surprising, since the scenario described here may be viewed as an extension of conventional ambient temporal monitoring methods, which estimate small velocity changes in a medium in the time-domain by stretching an ambient noise correlation function, thus in effect measuring a small change in frequency content, and therefore velocity (Brenguier et al., 2007).

Unlike lab experiments by Takei and Maeno (2004), we found that the shift downward was only partially reversed by a return to much colder temperatures, indicative of irreversible change through melting and/or compaction at our stations. The sites studied here responded rapidly to the first substantial decrease in atmospheric temperatures (at GIL) following the melt event (Figure 2c), in response to near-surface cooling/stiffening. This is consistent with rapid response of the top meter to changes in air temperature, and with the relative stability of lower frequency modes during this partial recovery period (Figure 3d). The response of the firn to air temperature changes occurred on a multiday time scale, which is much longer than the (hours) wind-related deposition scale and much shorter than the erosion sublimation time scale. This first-order response initially follows a predictable pattern (a substantial velocity decrease, similarly modeled in other ambient noise temporal monitoring scenarios, Minato et al., 2012), thus making this approach particularly well suited to melt detection. Whereas satellite-based observations are limited by orbital cycles and sparse measurements, this approach allows for direct structural interpretation of environmental forcing on extremely short time scales.

3. Conclusions

Firn-trapped seismic energy generated by ambient source processes was observed year-round on the RIS at frequencies >5 Hz. These signals were inverted for depth-dependent changes in local, near-surface elasticity and density at high temporal resolution (minutes to hours) using data from a single, continuously recording seismic station. Strong wind events produced both rapid (contemporaneous with high winds and dune formation) and slow (during interpreted subsequent dune erosion) spectral amplitude and frequency changes. The impact of wind events is distinctive and can be reliably discriminated from other environmental drivers when correlated with total spectral power and wind speed measurements. A separate environmental phenomenon was observed when air temperatures approached and subsequently exceeded the freezing point, during which a gradual downward shift of resonance peaks occurred. Modeling showed that this behavior is consistent with diffusion of a warm temperature anomaly to depth and corresponding softening and melt. For an unusually widespread and well-observed melt event in January 2016, a roughly 35–40% drop in firn seismic velocity to a depth of up to several meters was observed and modeled for multiple stations in central RIS within the melt event contour. The nonreversible nature of this response implied sensitivity of high-frequency seismic observations to long-term structural changes to the firn layer.

More refined three-component modeling of firn properties in a Biot theoretical (i.e., lattice and pore) framework (Sidler, 2015) is possible, and would benefit by utilizing extended data collected with easily deployable small (i.e., to tens of meters aperture) high-frequency seismic surface/shallow borehole arrays with collocated weather, video, ice core, and vertical temperature profile data. Such refined data and analysis would improve the process and structural understanding of surface and near-surface perturbations arising from storms and melt events, some of which may become more frequent in the future at more southerly ice shelves, such as the RIS. A similar methodology could also be applied to study the evolution of near-surface structure and state in response to environmental forcing in general firn-covered glacial systems.

Acknowledgments

JC was supported by Yates funds in the Colorado State University Department of Mathematics. DAW; RA, MB, and RE; and AN were supported under NSF Grants PLR-1142518, 1141916 and 1142126, respectively. PDB and PG were supported by NSF Grant PLR 1246151. RAS was supported by NSF Grant PLR-1246416. PDB also received support from the California Department of Parks and Recreation, Division of Boating and Waterways under contract 11-106-107. We thank Reinhard Flick and Patrick Shore for their support during field work and Tom Bolmer in locating stations and preparing maps and the US Antarctic Program for logistical support. The seismic instruments were provided by the Incorporated Research Institutions for Seismology (IRIS) through the PASSCAL Instrument Center at New Mexico Tech. Data collected are available through the IRIS Data Management Center under RIS and DRIS network code XH. The facilities of the IRIS Consortium are supported by the National Science Foundation under Cooperative Agreement EAR-1261681 and the DOE National Nuclear Security Administration. We thank Brad Lipovsky for his helpful internal review. The authors appreciate the support of the University of Wisconsin-Madison Automatic Weather Station Program for the data set, data display, and information, NSF grant number ANT-1543305.

References

Albert, D. G. (1998). Theoretical modeling of seismic noise propagation in firn at the South Pole, Antarctica. *Geophysical Research Letters*, *25*(23), 4257–4260.

Alley, K., Scambos, T., Anderson, R., Rajaram, H., Pope, A., & Haran, T. (2018). Continent-wide estimates of Antarctic strain rates from Landsat 8-derived velocity grids. *Journal of Glaciology*, *64*(244), 321–332. https://doi.org/10.1017/jog.2018.23

Alley, K., Scambos, T., Miller, J. Z., Long, D. G., & MacFerrin, M. (2018). Quantifying vulnerability of Antarctic ice shelves to hydrofracture using microwave scattering properties. *Remote Sensing of Environment*, *210*, 297–306. https://doi.org/10.1016/j.rse.2018.03.025

Alley, K., Scambos, T., Siegfried, M., & Fricker, H. (2016). Impacts of warm water on Antarctic ice shelf stability through basal channel formation. *Nature Geoscience*, *9*, 290–293.

Anthony, R., Aster, R., Wiens, D., Nyblade, A., Anandakrishnan, S., Huerta, A., et al. (2015). The seismic noise environment of Antarctica. *Seismological Research Letters*, *86*(1), 89–100.

Aster, R. C., Shearer, P. M., & Berger, J. (1990). Quantitative measurements of shear wave polarizations at the Anza seismic network, southern California: Implications for shear-wave splitting and earthquake prediction. *Journal of Geophysical Research*, *95*(B8), 12,449–12,473. https://doi.org/10.1029/JB095iB08p12449

Banwell, A. F., Willis, I. C., & Arnold, N. S. (2013). Modeling subglacial water routing at Paakitsoq, W Greenland. *Journal of Geophysical Research: Earth Surface*, *118*, 1282–1295. https://doi.org/10.1002/jgrf20093

Brenguier, F., Shapiro, N., Campillo, M., Ferrazzini, V., Duputel, Z., Coutant, O., et al. (2007). Toward forecasting volcanic eruptions using seismic noise. *Nature Geoscience*, *1*, 126–130.

Bromirski, P., Diez, A., Gerstoft, P., Stephen, R. A., Bolmer, T., Wiens, D., et al. (2015). Ross Ice Shelf vibrations. *Geophysical Research Letters*, *42*, 7589–7597. https://doi.org/10.1002/2015GL065284

Bromirski, P. D., Sergienko, O. V., & MacAyeal, D. R. (2010). Transoceanic infragravity waves impacting Antarctic ice shelves. *Geophysical Research Letters*, *37*, L02502. https://doi.org/10.1029/2009GL041488

Bromirski, P., & Stephen, R. (2012). Response of the Ross Ice Shelf, Antarctica, to ocean gravity-wave forcing. *Annals of Glaciology*, *53*(60), 163–172.

Bromwich, D., Liu, Z., Rogers, A. N., & Van Woert, M. (2013). Winter atmospheric forcing of the Ross Sea polynya. In S. S. Jacobs & R. F. Weiss (Eds.), *Ocean, ice, and atmosphere: Interactions at the Antarctic continental margin* (pp. 101–134). Washington, DC: American Geophysical Union. https://doi.org/10.1029/AR075p0101

Capelli, A., Kapil, J., Reiweger, I., Or, D., & Scheiwer, J. (2016). Speed and attenuation of acoustic waves in snow: Laboratory experiments and modeling with Biot's theory. *Cold Regions Science and Technology*, *125*, 1–11.

Cathles, L., Okal, E., & MacAyeal, D. (2009). Seismic observations of sea swell on the floating ross ice shelf, Antarctica. *Journal of Geophysical Research*, *114*, F02015. https://doi.org/10.1029/2007JF000934

Chen, Z., Bromirski, P., Gerstoft, P., Stephen, R., Wiens, D., Aster, R., et al. (2018). Ocean-excited plate waves in the Ross and Pine Island Glacier Ice Shelves. *Journal of Glaciology*, 1–15. https://doi.org/10.1017/jog.2018.66

Dadic, R., Mott, R., Horgan, H., & Lehning, M. (2013). Observations, theory, and modeling of the differential accumulation of Antarctic megadunes. *Journal of Geophysical Research: Earth Surface*, *118*, 2343–2353. https://doi.org/10.1002/2013JF002844

Diez, A., Bromirski, P. D., Gerstoft, P., Stephen, R. A., Anthony, R. E., Aster, R. C., et al. (2016). Ice shelf structure derived from dispersion curve analysis of ambient seismic noise, Ross Ice Shelf, Antarctica. *Geophysical Journal International*, *205*, 785–795.

Doake, C. S. M., Corr, H. F. J., Rott, H., Skvarca, P., & Young, N. (1998). Breakup and conditions for stability of the northern Larsen Ice Shelf, Antarctica. *Nature*, *391*, 778–780.

Ekaykin, A., Eberlein, L., Lipenkov, V., Popov, S., Scheinert, S., Schoder, L., et al. (2016). Non-climatic signal in ice core records: Lessons from Antarctic megadunes. *The Cryosphere*, *10*, 1217–1227. https://doi.org/10.5194/tc-10-1217-2016

Fetterer, F., Knowles, K., Meier, W., & Savoie, M. (2002). Sea ice index, National Snow and Ice Data Center. http://nsidc.org/data/g02135.html

Filhol, S., & Sturm, M. (2015). Snow bedforms: A review, new data, and a formation model. *Journal of Geophysical Research: Earth Surface*, *120*, 1645–1669. https://doi.org/10.1002/2015JF003529

Fretwell, P., Pritchard, H. D., Vaughan, D. G., Bamber, J. L., Barrand, N. E., Bell, R., et al. (2013). Bedmap2: Improved ice bed, surface and thickness datasets for Antarctica. *The Cryosphere*, *7*, 375–393.

Furst, J., Durand, G., Gillet-Chaulet, F., Tavard, L., Rankl, M., Braun, M., et al. (2016). *The safety band of Antarctic ice shelves*, vol. 6, pp. 479–482. https://doi.org/10.1038/NCLIMATE2912

Gilbert, A., Vincent, C., Six, D., Wagnon, P., Piard, L., & Ginot, P. (2014). Modeling near-surface firn temperature in a cold accumulation zone (Col du Dôme, French Alps): From a physical to a semi-parameterized approach. *The Cryosphere*, *8*, 689–703. https://doi.org/10.5194/tc-8-689-2014

Glushkov, E., Glushkova, N., & Chuanzeng, C. (2012). Surface and pseudo-surface acoustic waves piezoelectrically excited in diamond-based structures. *Journal of Applied Physics*, *112*, 064911.

Holland, P. R., Brisbourne, A., Corr, H. F. J., McGrath, D., Purdon, K., Paden, J., et al. (2015). Oceanic and atmospheric forcing of Larsen C Ice-Shelf thinning. *The Cryosphere*, *9*, 1005–1024. https://doi.org/10.5194/tc-9-1005-2015

Hubbard, B., Luckman, A., Ashmore, D., Bevan, S., Kulessa, B., Kuipers-Munneke, P., et al. (2016). Massive subsurface ice formed by refreezing of ice-shelf melt ponds. *Nature Communications*, *7*, 11897.

Hulbe, C., Scambos, T., Lee, C., Bohlander, J., & Haran, T. (2016). Recent changes in the flow of the Ross Ice Shelf, West Antarctica. *Earth and Planetary Science Letters*, *376*, 54–62.

Humbert, A., Greve, R., & Hutter, K. (2005). Parameter sensitivity studies for the ice flow of the Ross Ice Shelf, Antartica. *Journal of Geophysical Research*, *110*, F04022. https://doi.org/10.1029/2004JF000170

Kochanski, K., Anderson, R., & Tucker, G. (2018). Statistical classification of self-organized snow surfaces. *Geophysical Research Letters*, *45*, 6532–6541. https://doi.org/10.1029/2018GL077616

Kuipers Munneke, P., Ligtenberg, S. R. M., Van Den Broeke, M. R., & Vaughan, D. G. (2017). Firn air depletion as a precursor of Antarctic ice-shelf collapse. *Journal of Glaciology*, *60*(220), 205–214. https://doi.org/10.3189/2014JoG13J183

Kulessa, B., Jansen, D., Luckman, A. J., King, E. C., & Sammonds, P. R. (2014). Marine ice regulates the future stability of a large Antarctic ice shelf. *Nature Communications*, *5*, 3707. https://doi.org/10.1038/ncomms4707, https://www.nature.com/articles/ncomms4707supplementary-information

Kushibiki, J., Ishikawa, T., & Chubachi, N. (1990). Cut off characteristics of leaky Sezawa and pseudo-Sezawa wave modes for thin-film characterization. *Applied Physics Letters*, *57*(19). https://doi.org/10.1063/1.103982

Li, L., & Pomeroy, J. (1997). Probability of occurrence of blowing snow. *Journal of Geophysical Research*, *102*(D18), 21,955–21,964. https://doi.org/10.1029/97JD01522

Li, J., & Zwally, J. (2011). Modeling of firn compaction for estimating ice-sheet mass change from observed ice-sheet elevation change. *Annals of Glaciology*, *52*(59), 1–7.

MacAyeal, D. R., Okal, E. A., Aster, R. C., Bassis, J. N., Brunt, K. M., Cathles, L. M., et al. (2006). Transoceanic wave propagation links iceberg calving margins of Antarctica with storms in tropics and Northern Hemisphere. *Geophysical Research Letters*, *33*, L17502. https://doi.org/10.1029/2006GL027235

Marsh, O., Fricker, H. A., Siegfried, M., Christianson, K., Nicolls, K., Corr, H., et al. (2016). High basal melting forming a channel at the grounding line of Ross Ice Shelf, Antarctica. *Geophysical Research Letters*, *43*(1), 250–55. https://doi.org/10.1002/2015GL066612

Matthew, A. L., George, A. W., Linda, M. K., Jonathan, E. T., & John, J. C. (2012). Antarctic Automatic Weather Station program: 30 years of polar observation. *Bulletin of the American Meteorological Society*, *93*(10), 1519–1537. https://doi.org/10.1175/BAMS-D-11-00015.1

McGrath, D., Steffen, K., Rajaram, H., Scambos, T., Abdalati, W., & Rignot, E. (2012). Basal crevasses on the Larsen C Ice Shelf, Antarctica: Implications for meltwater ponding and hydrofracture. *Geophysical Research Letters*, *39*, l16504. https://doi.org/10.1029/2012GL052413

Minato, S., Tsuji, T., Ohmi, S., & Matsuoka, T. (2012). Monitoring seismic velocity change caused by the 2011 Tohoku-oki earthquake using ambient noise records. *Geophysical Research Letters*, *39*, L09309. https://doi.org/10.1029/2012GL051405

Mohanan, A., Islam, M. S., Ali, S. H., Parthiban, R., & Ramakrishnan, N. (2013). Investigation into mass loading sensitivity of Sezawa wave mode-based surface acoustic wave sensors. *Sensors*, *13*, 2164–2175.

Naish, T. e. t. (2009). Obliquity-paced Pliocene West Antarctic ice sheet oscillations. *Nature*, *458*, 322–328.

Nicolas, J., Vogelmann, A., Scott, R., Wilson, A., Cadeddu, M., & Bromwich, D. (2017). January 2016 extensive summer melt in West Antarctica favoured by strong El Niño. *Nature Communications*, *8*, 15799. https://doi.org/10.1038/ncomms15799

Paolo, F., Fricker, H., & Padman, L. (2015). Volume loss from Antarctic ice shelves is accelerating. *Science*, *348*(6232), 327–331.

Park, J., Lindberg, C., & Vernon, F. III (1987). Multitaper spectral analysis of high frequency seismograms. *Journal of Geophysical Research: Solid Earth*, *92*(B12), 12,675–12,684. https://doi.org/10.1029/JB092iB12p12675

Peterson, J. (1993). Observation and modeling of seismic background noise, US Geological Survey, Open Report pp. 93–322.

Piña-Flores, J., Perton, M., García-Jerez, A., Carmona, E., LuzÃsn, F., Molina-Villegas, J. C., et al. (2016). The inversion of spectral ratio H/V in a layered system using the diffuse field assumption (DFA). *Geophysical Journal International*, *208*(1). https://doi.org/10.1093/gji/ggw416

Pritchard, H. D., Ligtenberg, S. R. M., Fricker, H. A., Vaughan, D. G., van den Broeke, M. R., & Padman, L. (2012). Antarctic ice-sheet loss driven by basal melting of ice shelves. *Nature*, *484*, 502. https://doi.org/10.1038/nature10968, https://www.nature.com/articles/nature10968supplementary-information

Reeh, N. (2008). A nonsteady-state firn-densification model for the percolation zone of a glacier. *Journal of Geophysical Research*, *113*, F03023. https://doi.org/10.1029/2007JF000746

Reese, R., Gudmundsson, G., Levermann, A., & Winkelmann, R. (2018). The far reach of ice-shelf thinning in Antarctica. *Nature Climate Change*, *8*, 53–57.

Rignot, E., Casassa, G., Gogineni, P., Krabill, W., Rivera, A., & Thomas, R. (2004). Accelerated ice discharge from the Antarctic Peninsula following the collapse of Larsen B ice shelf. *Geophysical Research Letters*, *31*, LI8401. https://doi.org/10.1029/2004GL020697

Rignot, E., Jacobs, S., Mouginot, J., & Scheuch, B. (2013). Ice-shelf melting around Antarctica. *Science*, *341*(6143), 266–270.

Rodriguez-Madrid, J., Iriarte, G. F., Pedros, J., Williams, O. A., Brink, D., & Calle, F. (2012). Super-high-frequency SAW resonators on AlN/diamond. *IEEE Electron Device Letters*, *33*(4), 495–497.

Scambos, T. A., Bohlander, J. A., Shuman, C. A., & Skvarca, P. (2004). Glacier acceleration and thinning after ice shelf collapse in the Larsen B embayment, Antarctica. *Geophysical Research Letters*, *31*, L18402. https://doi.org/10.1029/2004GL020670

Scambos, T., Fricker, H. A., Liu, C.-C., Bohlander, J., Fastook, J., Sargent, A., et al. (2009). Ice shelf disintegration by plate bending and hydro-fracture: Satellite observations and model results of the 2008 Wilkins ice shelf break-ups. *Earth and Planetary Science Letters*, *280*(1-4), 51–60.

Schmidt, H., & Jensen, F. B. (1985). A full wave solution for propagation in multilayered viscoelastic media with application to Gaussian beam reflection at fluid-solid interfaces. *The Journal of the Acoustical Society of America*, *77*(3), 813–825. https://doi.org/10.1121/1.392050

Sergienko, O. (2010). Elastic response of floating glacier ice to long-period ocean waves. *Journal of Geophysical Research*, *115*, F04028. https://doi.org/10.1029/2010JF001721

Shepherd, A. (2018). The IMBIE team Mass balance of the Antarctic ice sheet from 1992 to 2017. *Nature*, *558*, 219–222.

Sidler, R. (2015). A porosity-based Biot model for acoustic waves in snow. *Journal of Glaciology*, *61*(228).

Sommer, C., Wever, N., Fierz, C., & Lehning, M. (2018). Wind-packing of snow in Antarctica. *The Cryosphere*, 36. https://doi.org/10.5194/tc-2018-36

Stahler, S. C., Panning Mark, P., Vance Steven, D., Lorenz Ralph, D., vanDriel, M., Nissen-Meyer, T., et al. (2017). Seismic wave propagation in icy ocean worlds. *Journal of Geophysical Research: Planets*, *123*(1), 206–232. https://doi.org/10.1002/2017JE005338

Takei, I., & Maeno, N. (2004). Mechanical vibration responses of snow samples near the melting temperature. *Annals of Glaciology*, *38*, 130–134.

Van Lipzip, N., King, J., Lachlan-Cope, T., & Van den Broeke, M. (2004). Precipitation, sublimation, and snow drift in the Antarctic Peninsula region from a regional atmospheric model. *Journal of Geophysical Research*, *109*, D24106. https://doi.org/10.1029/2004JD004701

Van den Broeke, M. (1997). Spatial and temporal variation of sublimation on Antarctica: Results of a high-resolution general circulation model. *Journal of Geophysical Research*, *102*, 29,765–29,777.

Walker, C., Bassis, J. N., Fricker, H. A., & Czerwinski, R. J. (2013). Structural and environmental controls on Antarctic ice shelf rift propagation inferred from satellite monitoring. *Journal of Geophysical Research: Earth Surface*, *118*, 2354–2364. https://doi.org/10.1002/2013JF002742

Xie, D., & Farmer, Y. (1994). Seismic-acoustic sensing of sea ice wave mechanical properties. *Journal of Geophysical Research*, *99*(C4), 7771–7786.

Zhan, Z., Tsai, V. C., Jackson, J., & Helmberger, D. (2014). Ambient noise correlation on the Amery Ice Shelf, East Antarctica. *Geophysical Journal International*, *196*(3), 1796–1802. https://doi.org/10.1093/gji/ggt488